

Dissipative Topological Phase Transition with Strong System-Environment Coupling

Wei Nie,¹ Mauro Antezza^{2,3}, Yu-xi Liu^{4,5,*} and Franco Nori^{1,6,7,†}¹Theoretical Quantum Physics Laboratory, RIKEN Cluster for Pioneering Research, Wako-shi, Saitama 351-0198, Japan²Laboratoire Charles Coulomb (L2C), UMR 5221 CNRS-Université de Montpellier, F- 34095 Montpellier, France³Institut Universitaire de France, 1 rue Descartes, F-75231 Paris Cedex 05, France⁴School of Integrated Circuits, Tsinghua University, Beijing 100084, China⁵Frontier Science Center for Quantum Information, Beijing, China⁶RIKEN Center for Quantum Computing (RQC), 2-1 Hirosawa, Wako-shi, Saitama 351-0198, Japan⁷Physics Department, The University of Michigan, Ann Arbor, Michigan 48109-1040, USA (Received 1 April 2021; revised 20 July 2021; accepted 1 November 2021; published 14 December 2021)

A primary motivation for studying topological matter regards the protection of topological order from its environment. In this work, we study a topological emitter array coupled to an electromagnetic environment. The photon-emitter coupling produces nonlocal interactions between emitters. Using periodic boundary conditions for all ranges of environment-induced interactions, the chiral symmetry inherent to the emitter array is preserved. This chiral symmetry protects the Hamiltonian and induces parity in the Lindblad operator. A topological phase transition occurs at a critical photon-emitter coupling related to the energy spectrum width of the emitter array. Interestingly, the critical point nontrivially changes the dissipation rates of edge states, yielding a dissipative topological phase transition. In the protected topological phase, edge states suffer from environment-induced dissipation for weak photon-emitter coupling. However, strong coupling leads to robust dissipationless edge states with a window at the emitter spacing. Our work shows the potential to manipulate topological quantum matter with electromagnetic environments.

DOI: [10.1103/PhysRevLett.127.250402](https://doi.org/10.1103/PhysRevLett.127.250402)

Introduction.—Vacuum electromagnetic environments can nontrivially change order parameters of matter, producing phase transitions [1,2]. With the advances in cavity quantum electrodynamics (QED) [3–6], vacuum electromagnetic fields are used to manipulate matter [7–10] with strong light-matter interaction. For example, in cavity-interfaced superconductors, a strong coupling with electromagnetic fields changes the superconducting transition temperature [9]. Recently, the vacuum electromagnetic control of matter is receiving growing attention [11–13]. Due to symmetry-protected properties, topological matter is also being studied in the coupling with electromagnetic fields for potential applications [14–16]. The band gap of a kagome metasurface of dipole emitters embedded in a cavity can be tuned by electromagnetic fields [17]. Varying the cavity width can change long-range interactions between emitters and induce topological phase transitions [16].

A prerequisite to make topological protection reliable is to understand dissipative properties of topological systems [18–33]. Energy bands play a pivotal role for topological matter, e.g., in studying topological phases [34–37] and topological criticalities [38–40]. The large gap between energy bands protects topological properties from local disorder [41–49] and thermal noises [50–55]. However, a recent study [56] of time-reversal symmetry protected topological systems with large band gap shows the fragility

of topological phases in electromagnetic environments. Via *perturbation* theory, they find that quantum coherence between edge states in one-dimensional (1D) topological systems is spoiled when system-environment coupling is weak compared to the band gap. This finding shows the challenge of protecting topological quantum matter in electromagnetic environments.

In this work, we study the coupling between a topological emitter array and its electromagnetic environment in the *nonperturbative* regime, i.e., edge states are coupled to bulk states via the environment. We find that for emitter spacings $d = \lambda_0/4$ and $d = 3\lambda_0/4$, environment-induced interactions have chiral symmetry and produce distinct topological phases. For $d = \lambda_0/4$, environment modifies the topological phase with dissipative edge states. However, the edge states for $d = 3\lambda_0/4$ are protected from dissipation in a parameter space specified by the Lindblad operator. In the thermodynamic limit, a dissipative topological phase transition (DTPT), characterized by a nontrivial change of dissipation of the edge states, occurs at $d = 3\lambda_0/4$ when the single-emitter decay rate induced by the system-environment coupling equals the energy spectrum width of the topological emitter array. These results could be useful for improving topological protection in open quantum systems which have nonlocal dissipations [56].

One-dimensional topological emitter array in vacuum electromagnetic fields.—We consider a topological array of dipole emitters coupled to its surrounding electromagnetic

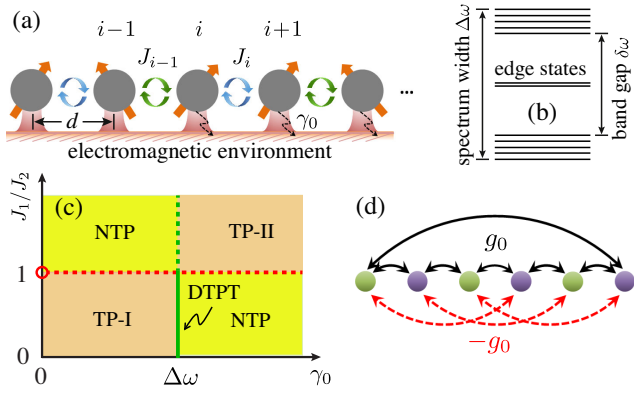


FIG. 1. (a) Schematic of a topological emitter array coupled to an electromagnetic environment. Emitters have nearest-neighbor interactions J_i , homogeneous spacing d , and decay rate γ_0 to the environment. (b) Single-excitation spectrum of the topological system with spectrum width $\Delta\omega$ and band gap $\delta\omega$. (c) Phase diagram of the system for emitter spacing $d = 3\lambda_0/4$. There are topological phases TP-I (having edge states), TP-II (having no edge state), and nontopological phase (NTP). The red circle at $(\gamma_0 = 0, J_1/J_2 = 1)$ represents the original phase transition in the SSH model. The horizontal red dashed line denotes the SSH-type phase transition in the dissipative regime. The vertical green line represents the environment-induced topological phase transition where the decay rate γ_0 is equal to the spectrum width $\Delta\omega$ of the topological system. In particular, the green solid line indicates the dissipative topological phase transition. (d) Photon-mediated interactions H_{ph} for $d = \lambda_0/4$ ($g_0 = \gamma_0/2$) and $d = 3\lambda_0/4$ ($g_0 = -\gamma_0/2$).

environment, as in Fig. 1(a). The single-excitation energy spectrum of the topological emitter array with band gap and spectrum width is shown in Fig. 1(b). Electromagnetic modes in the environment are described by $H_E = \int d^3\mathbf{r} \int_0^\infty d\omega \hbar\omega \hat{a}^\dagger(\mathbf{r}, \omega) \hat{a}(\mathbf{r}, \omega)$, where $\hat{a}^\dagger(\mathbf{r}, \omega)$ and $\hat{a}(\mathbf{r}, \omega)$ are the creation and annihilation operators of photons. The emitter-environment coupling is $H_{\text{int}} = -\sum_i \int_0^\infty d\omega (\hat{\mathbf{d}}_i \cdot \mathbf{E}(\mathbf{r}_i, \omega) + \text{H.c.})$, where $\hat{\mathbf{d}}_i = \mathbf{d}_i \sigma_i^- + \mathbf{d}_i^* \sigma_i^+$ is the dipole moment operator of the i th emitter. The electric field operator is $\mathbf{E}(\mathbf{r}, \omega) = i\eta \int d^3\mathbf{r}' \sqrt{\epsilon_I(\mathbf{r}', \omega)} \mathbf{G}(\mathbf{r}, \mathbf{r}', \omega) \hat{a}(\mathbf{r}', \omega)$, where $\eta = \sqrt{\hbar\omega^2 / \sqrt{\pi\epsilon_0} c^2}$; $\epsilon_I(\mathbf{r}', \omega)$ is the imaginary part of the complex permittivity; the Green's tensor $\mathbf{G}(\mathbf{r}, \mathbf{r}', \omega)$ describes the electromagnetic interaction from \mathbf{r}' to \mathbf{r} . The dynamics of the topological emitter array is described by the master equation [57,58]

$$\dot{\rho}(t) = -\frac{i}{\hbar} [H_0 + H_{\text{topo}} + H_{\text{ph}}, \rho(t)] + \mathcal{D}[\rho], \quad (1)$$

where the free energy is $H_0 = \sum_i \hbar\omega_0 \sigma_i^+ \sigma_i^-$ (ω_0 is the transition frequency of emitters) and the topological emitter array is described by $H_{\text{topo}} = \sum_i \hbar J_i (\sigma_i^+ \sigma_{i+1}^- + \sigma_{i+1}^+ \sigma_i^-)$ with tunable dimerized interactions $J_i = J_0 [1 + (-1)^i \cos\varphi]$ [59]. The emitter-environment coupling can be strong

compared with the band gap, but much smaller than the energy of emitters, to satisfy the Born-Markov approximation in Eq. (1). The virtual-photon exchange between emitters and environment yields $H_{\text{ph}} = \sum_{i,j=1}^N \hbar g_{ij} (\sigma_i^- \sigma_j^+ + \sigma_j^- \sigma_i^+)$, where g_{ij} [Eq. (3)] characterize the strengths of the nonlocal dipole-dipole interactions. In addition to the coherent part H_{ph} , the virtual-photon exchange yields correlated dissipations γ_{ij} [Eq. (4)], which are included in the Lindblad operator,

$$\mathcal{D}[\rho] = \sum_{i,j=1}^N \gamma_{ij} \left(\sigma_i^- \rho \sigma_j^+ - \frac{1}{2} \sigma_i^+ \sigma_j^- \rho - \frac{1}{2} \rho \sigma_i^+ \sigma_j^- \right). \quad (2)$$

By applying the Kramers-Kronig relation to the Green's tensor and integrating in the frequency domain, the photon-mediated interactions and dissipations become [60–69]

$$g_{ij} = \frac{\omega_0^2}{\hbar\epsilon_0 c^2} \text{Re}[\mathbf{d}_i^* \cdot \mathbf{G}(\mathbf{r}_i, \mathbf{r}_j, \omega_0) \cdot \mathbf{d}_j], \quad (3)$$

$$\gamma_{ij} = \frac{2\omega_0^2}{\hbar\epsilon_0 c^2} \text{Im}[\mathbf{d}_i^* \cdot \mathbf{G}(\mathbf{r}_i, \mathbf{r}_j, \omega_0) \cdot \mathbf{d}_j]. \quad (4)$$

For the 1D electromagnetic environment, concrete forms of the nonlocal interactions and correlated dissipations are [63,64,70–74] $g_{ij} = \gamma_0 \sin(2\pi d_{ij}/\lambda_0)/2$ and $\gamma_{ij} = \gamma_0 \cos(2\pi d_{ij}/\lambda_0)$, respectively. Here, the emitter decay rate is $\gamma_0 = g^2/c$ where g is the photon-emitter coupling and c is the group velocity of photons; d_{ij} is the distance between i th and j th emitters; λ_0 is the wavelength of a photon with frequency ω_0 . We find that the *spectrum width* $\Delta\omega$ sets a critical point for a dissipation-induced topological phase transition, represented by the green solid vertical line in Fig. 1(c).

Environment-protected chiral symmetry.—As a simple illustration, in Fig. 1(d) the environment induces nearest-neighbor (NN) and long-range interactions in an array with $N = 6$ emitters. We consider the cases when the spacings $d = \lambda_0/4$ and $d = 3\lambda_0/4$; and the parameter g_0 is $\gamma_0/2$ and $-\gamma_0/2$, respectively. The long-range interaction between the first and the last emitters provides periodic boundary conditions for the NN interaction. Conversely, the long-range interaction between the i th and $(i+5)$ th emitters exhibits translational invariance due to the NN interaction. Therefore, the effective strengths for the NN interaction and the long-range interaction between the i th and $(i+5)$ th emitters are $g_0/2$. Moreover, the effective interaction g_{ij} between the i th and $(i+3)$ th emitters (red dashed curves) is $-g_0/2$. With this protocol, the translational symmetry is preserved for all ranges of interactions induced by the environment at $d = \lambda_0/4$ and $d = 3\lambda_0/4$. However, for other values of the spacing d , the translational symmetry in H_{ph} is broken.

By assuming periodic boundary conditions on H_{topo} , the coherent interaction $H = H_{\text{topo}} + H_{\text{ph}}$ in quasimomentum space is $H/\hbar = \sum_k \Psi_k^+ \mathcal{H}(k) \Psi_k$, where $\Psi_k^+ = (\sigma_{A,k}^+, \sigma_{B,k}^+)$. Here, A and B denote odd- and even-site emitters, respectively. The 1D symmetry-protected topological system is described by the Su-Schrieffer-Heeger (SSH) model [75]. In the sublattice space, we obtain an effective spin-1/2 Hamiltonian $\mathcal{H}(k) = h_x(k)\tau_x + h_y(k)\tau_y$ with chiral symmetry $\tau_z \mathcal{H}(k) \tau_z = -\mathcal{H}(k)$ [76]. Here, τ_x, τ_y, τ_z are Pauli matrices, and

$$h_x(k) = J_1 + J_2 \cos(k) + \frac{g_0}{2} \left[1 + \cos\left(\frac{Nk}{2}\right) \right], \quad (5)$$

$$h_y(k) = J_2 \sin(k) + \frac{g_0}{2} \mathcal{F}(k), \quad (6)$$

with $g_0 = \gamma_0/2$ ($-\gamma_0/2$) for $d = \lambda_0/4$ ($3\lambda_0/4$), $\mathcal{F}(k) = \sum_{j=1}^{N/2} 2(-1)^{j-1} \sin(jk) - \sin(Nk/2)$, and energy bands $\varepsilon_{\pm}(k) = \pm \sqrt{h_x^2(k) + h_y^2(k)}$. Without the environment, the energy bands are shown in Fig. 2(a). The band gap and spectrum width are

$$\delta\omega = 2|J_1 - J_2|, \quad \Delta\omega = 2(J_1 + J_2), \quad (7)$$

respectively. The dimerized interactions $J_{1,2} = J_0(1 \mp \cos\varphi)$ yield the band gap $\delta\omega = 4J_0 \cos\varphi$ and spectrum width $\Delta\omega = 4J_0$. The SSH-type topological phase transition takes

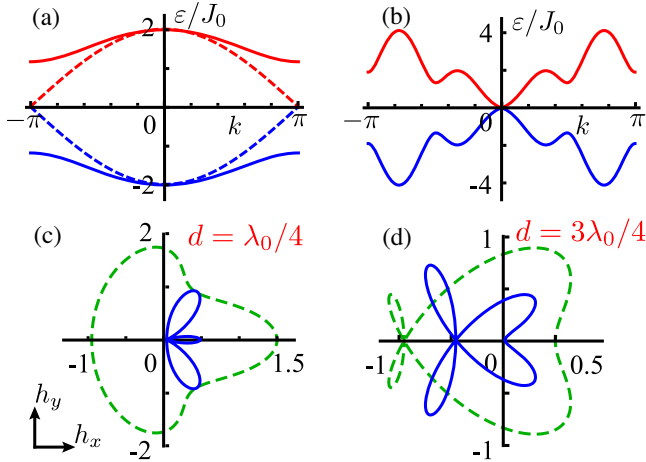


FIG. 2. (a) Energy bands of the topological emitter array for $J_1 \neq J_2$ (solid) and $J_1 = J_2$ (dashed). (b) Environment-induced gap closing at emitter spacing $d = 3\lambda_0/4$ and decay rate $\gamma_0 = \Delta\omega$. Topologies from the hybridization between H_{topo} and H_{ph} in auxiliary space $[h_x(k), h_y(k)]$ for (c) $d = \lambda_0/4$, and (d) $d = 3\lambda_0/4$. (c) The winding number is zero at $J_0 = 0$ (blue solid), and becomes one for $J_0 > 0$ (green dashed). (d) The winding number is zero for $0 \leq J_0 \leq \gamma_0/4$ (the blue solid topology denotes $J_0 = \gamma_0/4$), and becomes one for $J_0 > \gamma_0/4$ (green dashed). We consider $\varphi = 0.1\pi$, $N = 6$.

place at $k = \pm\pi$ [76] with linear low-energy dispersion. In the electromagnetic environment with emitter spacing $d = 3\lambda_0/4$, the condition

$$\gamma_0 = \Delta\omega, \quad (8)$$

yields a gap closing at $k = 0$ with parabolic dispersion, as shown in Fig. 2(b). The parabolic dispersion [38,39] makes this topological criticality to be different from the one in the SSH model. In the auxiliary space $[h_x(k), h_y(k)]$, the winding number can be defined as $W = (1/2\pi) \int_{\text{B.Z.}} d\theta_k$, with $\theta_k = \arctan[-h_x(k)/h_y(k)]$. For $d = \lambda_0/4$, shown in Fig. 2(c), the system is in a nontopological phase with $W = 0$ at $J_0 = 0$. However, as J_0 is increased, the winding number $W = 1$; i.e., the topological phase is protected when $d = \lambda_0/4$. For $d = 3\lambda_0/4$, in Fig. 2(d), the system has zero winding number for small J_0/γ_0 . However, at a critical point $\gamma_0^c = \Delta\omega$, a topological phase transition takes place. For $\gamma_0 < \gamma_0^c$, the system becomes topological with winding number $W = 1$. Namely, the topological phase is preserved when the spectrum width $\Delta\omega$ is larger than the environment-induced decay γ_0 of the emitters, as shown in Fig. 1(c).

Edge state vs dissipative topological phase transition.— Figures 3(a) and 3(b) show the energy spectra of H versus J_0/γ_0 for (a) $d = \lambda_0/4$ and (b) $d = 3\lambda_0/4$ in a system with an odd number of emitters $N = 21$, where a single edge state appears. In agreement with the topologies in quasimomentum space for these two emitter spacings, a band gap [3(a)] and a band touching [3(b)] are found. In Fig. 3(b), a nontopological edge state is found for the topologically trivial phase. Figures 3(c) and 3(d) show the

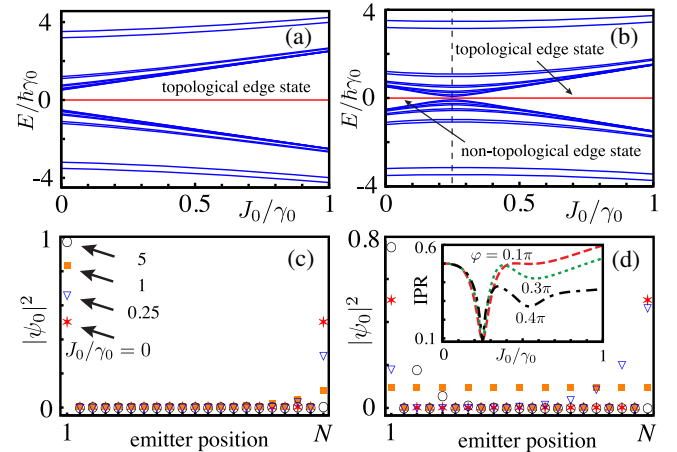


FIG. 3. Energy spectra for (a) $d = \lambda_0/4$, and (b) $d = 3\lambda_0/4$, respectively. Probability distribution $|\psi_0|^2$ of the zero-energy state for (c) $d = \lambda_0/4$ and (d) $d = 3\lambda_0/4$. In (c),(d), red stars, blue triangles, orange squares, and black circles correspond to $J_0/\gamma_0 = 0, 0.25, 1, 5$, and $J_0/\gamma_0 = 0, 0.2, 0.25, 1$, respectively. The inset of (d) shows the IPR of the zero-energy state at different values of φ for $d = 3\lambda_0/4$. In (a)–(d) we consider $\varphi = 0.1\pi$, $N = 21$.

distributions $|\psi_0|^2$ of the edge state. At $J_0 = 0$, the edge state is equally distributed at the two edge emitters with wave function $|\psi_0\rangle = (1/\sqrt{2})(\sigma_1^+ + \sigma_N^+)|G\rangle$, where $|G\rangle$ is the ground state of the emitter array. In Fig. 3(c), with $d = \lambda_0/4$, enlarging J_0 monotonically increases the component of $|\psi_0|^2$ at the left boundary. However, before the critical point, the left-boundary component of the edge state for $d = 3\lambda_0/4$ becomes smaller as J_0/γ_0 is increased. At the critical point, the gap of the spectrum closes and the edge state becomes delocalized. By further increasing J_0 , the edge state eventually localizes at the left boundary.

To characterize the changes of the edge state, we study the inverse participation ratio (IPR) [77], $\text{IPR} = \sum_i |\psi_{0i}|^4 / (\sum_i |\psi_{0i}|^2)^2$, where ψ_{0i} is the amplitude of the edge state at the i th emitter. In the inset of Fig. 3(d), we show the IPR versus J_0/γ_0 for $d = 3\lambda_0/4$. The IPR of the edge state at $J_0 = 0$ is one half due to its equal distribution at two boundaries. A minimum is found at the critical point for different values of φ , indicating the edge-bulk transition.

To study the stability of topological features in real space, we here rewrite the Lindblad operator in terms of eigenstates of H ,

$$\mathcal{D}[\rho] = \sum_{m,n} \Gamma_{mn} [\Psi_m^- \rho \Psi_n^+ - \frac{1}{2} \Psi_m^+ \Psi_n^- \rho - \frac{1}{2} \rho \Psi_m^+ \Psi_n^-], \quad (9)$$

with $\Psi_m^+ = |\Psi_m\rangle\langle G|$. Here, $|\Psi_m\rangle$ denotes the m th eigenmode of H . The decay rates are $\Gamma_{mn} = \sum_{i,j} \gamma_{ij} \langle e_i | \Psi_m \rangle \langle \Psi_n | e_j \rangle$, with $|e_i\rangle = \sigma_i^+ |G\rangle$. Specifically, Γ_{mm} denotes the decay rate of the m th eigenstate to environment; Γ_{mn} is the correlated decay from the n th state to m th state. The dissipation of the edge state is governed by Γ_{m0} . In Fig. 4(a), we show the scaled decay rate Γ_{00}/γ_0 from edge state to environment versus J_0/γ_0 . For $d = \lambda_0/4$, Γ_{00}/γ_0 increases with J_0/γ_0 , and decreases after reaching the maximum [58]. However, the edge state at $d = 3\lambda_0/4$ has a decay rate that decreases in the nontopological phase and that stops decaying at $J_0 = \gamma_0/4$. In finite systems, the weak emitter-environment coupling, i.e., small γ_0/J_0 , introduces dissipation of the edge state [58], which is responsible for the enhanced photon absorption [78]. However, the edge state for strong coupling is protected against decoherence in the topological phase.

For added clarity, the correlated decays Γ_{m0} ($m \neq 0$) between the edge state and the bulk states are shown in Fig. 4(b). At $J_0/\gamma_0 = 0.2$ (blue dots) in the nontopological phase, the edge state not only decays into the environment ($\Gamma_{00} \neq 0$), but also decays into the bulk states of the emitter array. However, at $J_0/\gamma_0 = 0.3$ (red squares) in the topological phase, the edge state does not decay to bulk states. At the critical point $J_0/\gamma_0 = 0.25$, the dissipations to bulk states are greatly suppressed, except for those of the two bulk states $m' = \pm(N-3)/2$. Near the critical point, the correlated dissipations $|\Gamma_{m'0}| \propto \exp(-\nu_{m'}N)$, with $\nu_{m'} > 0$

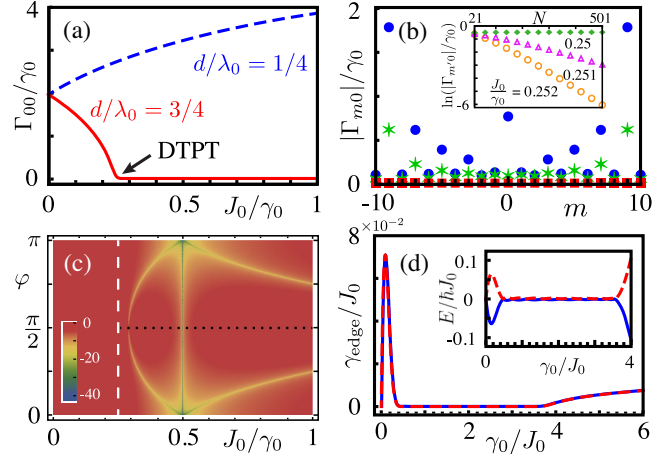


FIG. 4. (a) Dissipation Γ_{00} from edge state to environment for $d = \lambda_0/4$ (blue dashed) and $d = 3\lambda_0/4$ (red solid). (b) Dissipations Γ_{m0} from edge state to environment ($m = 0$) and bulk states ($m \neq 0$) for $d = 3\lambda_0/4$ at $J_0/\gamma_0 = 0.2$ (blue dots), 0.25 (green stars) and 0.3 (red squares). The inset shows $\ln(|\Gamma_{m'0}|/\gamma_0)$ versus N for $J_0/\gamma_0 = 0.25$ (green diamonds), 0.251 (purple triangles) and 0.252 (orange circles). (c) $\ln(\Gamma_{00}/\gamma_0)$ for the emitter array with $N = 7$. The white-dashed vertical ($J_0/\gamma_0 = 1/4$) and black-dotted horizontal lines indicate the DTPT and the SSH-type criticality, respectively. (d) Dissipations from edge states to environment. The inset shows the corresponding energy levels of the edge states. We consider $N = 21$ (one edge state) in (a),(b), $N = 20$ (two edge states) in (d); $\varphi = 0.3\pi$ in (a),(b),(d).

in the topological phase. The inset shows $\ln(|\Gamma_{m'0}|/\gamma_0)$ versus N . The values of $\nu_{m'}$ are 0, 0.005, and 0.0115, for $J_0/\gamma_0 = 0.25, 0.251, \text{ and } 0.252$, respectively. Therefore, in the thermodynamic limit $N \rightarrow +\infty$, the critical point indicates a transition between dissipative and dissipationless edge states, namely, a DTPT, which can be accessed by observing the population dynamics of the emitter array [58]. In Fig. 4(c), the local minima of $\ln(\Gamma_{00}/\gamma_0)$ show the parameter space of edge states protected by the Lindblad operator [79–82] in a small system. This protection is actually attributed to the vanishing overlap between edge states and polarized radiating modes in the Lindblad operator, which exhibits parity property, i.e., dissipations only occur between odd-site (even-site) emitters. Larger systems have broader parameter space for dissipationless edge states [58]. In particular, the condition that the environment-induced decay is half of the spectrum width, i.e., $J_0/\gamma_0 = 1/2$, produces a dissipationless edge state

$$\left| \psi_0 \left(\frac{J_0}{\gamma_0} \rightarrow \frac{1}{2} \right) \right\rangle = \frac{1}{\sqrt{N}} \sum_{n \in \mathbb{N}} (-1)^n \left(\tan \frac{\varphi}{2} \right)^{2n} |\psi\rangle_n, \quad (10)$$

for various localization lengths even near the SSH criticality. Here, $|\psi\rangle_n = (\sigma_{4n+1}^+ + \sigma_{4n+3}^+)|G\rangle$; namely, the $(4n+1)$ th and $(4n+3)$ th emitters have the same amplitude.

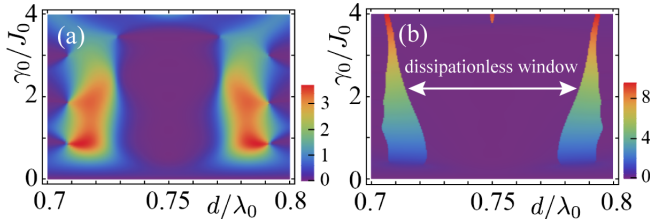


FIG. 5. (a) Decay rate Γ_{00} from edge state to environment. (b) Effective decay rate $\tilde{\Gamma}_0$ of edge state. Here, we consider $N = 11$, $\varphi = 0.3\pi$, $d = 3\lambda_0/4$.

Dissipationless subspace of topological edge states.—In arrays with an even number of emitters, two edge states appear at the boundaries. Figure 4(d) shows the decay rates and energy splitting (in the inset) of the edge states. With small γ_0 (weak coupling), the two localized edge states are coupled by environment-mediated long-range interactions, and the subspace of edge states suffers from decoherence [56,83]. Surprisingly, when the emitter-environment coupling is strong, i.e., γ_0 is large, the edge states are decoupled from each other. Therefore, they are both protected from dissipation until the DTPT at $\gamma_0 = \Delta\omega$. Moreover, strong coupling makes the zero splitting between edge states insensitive to emitter spacing around $d = 3\lambda_0/4$ [58].

Dissipationless window.—In Fig. 5(a), we show the dissipation Γ_{00} of a single edge state versus d/λ_0 . Even though the chiral symmetry is broken for emitter spacings around $3\lambda_0/4$, the edge state can be dissipationless and is insensitive to emitter spacing. To confirm this conjecture, we rewrite the whole system as a non-Hermitian effective Hamiltonian in the diagonalized form $H_{\text{eff}} = \sum_j (\tilde{E}_j - i\tilde{\Gamma}_j) |\tilde{\Psi}_j^R\rangle \langle \tilde{\Psi}_j^L|$ with the biorthogonal basis $\langle \tilde{\Psi}_j^L | \tilde{\Psi}_j^R \rangle = \delta_{jj}$. A dissipationless window is found for $d = 3\lambda_0/4$ with strong system-environment coupling, as shown in Fig. 5(b). This window makes the dissipationless edge state robust to disorder in emitter positions [58]. The edge state has finite decay rate around $d = \lambda_0/4$. For emitter spacings $n\lambda_0/2$ ($n = 0, 1, 2, \dots$) where H_{ph} is zero, the edge state is more dissipative and shows higher sensitivity to disorder than $d = 3\lambda_0/4$ [58].

Conclusions.—System-environment interplay is fundamental for dissipative topological matter. In this work, we show that a 1D topological emitter array globally coupled to an electromagnetic environment exhibits interesting dissipative properties as the system-environment coupling varies. The energy spectrum width of the emitter array sets a critical value for the system-environment coupling and produces the DTPT. The environment-modified topological edge states are stable and robust due to a dissipationless window in the emitter spacing. Our work paves an avenue for electromagnetic control of topological matter with vacuum fields.

We thank Christian Leefmans, Guo-Zhu Song, Clemens Gneiting, and Yanming Che for critical readings and insightful comments. Y.X.L. is supported by the National Basic Research Program (973) of China under Grant No. 2017YFA0304304, the Key-Area Research and Development Program of Guangdong Province under Grant No. 2018B030326001, and NSFC under Grant No. 11874037. F.N. is supported in part by Nippon Telegraph and Telephone Corporation (NTT) Research, Japan Science, and Technology Agency (JST) (via the Quantum Leap Flagship Program (Q-LEAP), Moonshot R&D Grant No. JPMJMS2061, and the Centers of Research Excellence in Science and Technology (CREST) Grant No. JPMJCR1676), Japan Society for the Promotion of Science (JSPS) (via the Grants-in-Aid for Scientific Research (KAKENHI) Grant No. JP20H00134, and the JSPS-RFBR Grant No. JPJSBP120194828), Army Research Office (ARO) (Grant No. W911NF-18-1-0358), the Asian Office of Aerospace Research and Development (AOARD) (via Grant No. FA2386-20-1-4069), and the Foundational Questions Institute (FQXi) (via Grant No. FQXi-IAF19-06).

*yuxiliu@mail.tsinghua.edu.cn

†fnori@riken.jp

- [1] R. Landig, L. Hruby, N. Dogra, M. Landini, R. Mottl, T. Donner, and T. Esslinger, Quantum phases from competing short- and long-range interactions in an optical lattice, *Nature (London)* **532**, 476 (2016).
- [2] Y. Ashida, A. İmamoğlu, J. Faist, D. Jaksch, A. Cavigliari, and E. Demler, Quantum Electrodynamical Control of Matter: Cavity-Enhanced Ferroelectric Phase Transition, *Phys. Rev. X* **10**, 041027 (2020).
- [3] S. Haroche and J.-M. Raimond, *Exploring the Quantum: Atoms, Cavities, and Photons* (Oxford University Press, New York, 2006).
- [4] X. Gu, A. F. Kockum, A. Miranowicz, Y.-X. Liu, and F. Nori, Microwave photonics with superconducting quantum circuits, *Phys. Rep.* **718–719**, 1 (2017).
- [5] A. F. Kockum, A. Miranowicz, S. De Liberato, S. Savasta, and F. Nori, Ultrastrong coupling between light and matter, *Nat. Rev. Phys.* **1**, 19 (2019).
- [6] F. Mivehvar, F. Piazza, T. Donner, and H. Ritsch, Cavity QED with quantum gases: New paradigms in many-body physics, *arXiv:2102.04473*.
- [7] F. Schlawin, A. Cavigliari, and D. Jaksch, Cavity-Mediated Electron-Photon Superconductivity, *Phys. Rev. Lett.* **122**, 133602 (2019).
- [8] J. B. Curtis, Z. M. Raines, A. A. Allocca, M. Hafezi, and V. M. Galitski, Cavity Quantum Eliashberg Enhancement of Superconductivity, *Phys. Rev. Lett.* **122**, 167002 (2019).
- [9] A. Thomas, E. Devaux, K. Nagarajan, T. Chervy, M. Seidel, D. Hagenmüller, S. Schütz, J. Schachenmayer, C. Genet, G. Pupillo, and T. W. Ebbesen, Exploring superconductivity under strong coupling with the vacuum electromagnetic field, *arXiv:1911.01459*.

- [10] F. J. Garcia-Vidal, C. Ciuti, and T. W. Ebbesen, Manipulating matter by strong coupling to vacuum fields, *Science* **373**, eabd0336 (2021).
- [11] A. González-Tudela, C.-L. Hung, D. E. Chang, J. I. Cirac, and H. Kimble, Subwavelength vacuum lattices and atom-atom interactions in two-dimensional photonic crystals, *Nat. Photonics* **9**, 320 (2015).
- [12] J. Perczel, J. Borregaard, D. E. Chang, S. F. Yelin, and M. D. Lukin, Topological Quantum Optics Using Atomlike Emitter Arrays Coupled to Photonic Crystals, *Phys. Rev. Lett.* **124**, 083603 (2020).
- [13] J. Rui, D. Wei, A. Rubio-Abadal, S. Hollerith, J. Zeiher, D. M. Stamper-Kurn, C. Gross, and I. Bloch, A subradiant optical mirror formed by a single structured atomic layer, *Nature (London)* **583**, 369 (2020).
- [14] M. Trif and P. Simon, Braiding of Majorana Fermions in a Cavity, *Phys. Rev. Lett.* **122**, 236803 (2019).
- [15] W. Nie and Y.-X. Liu, Bandgap-assisted quantum control of topological edge states in a cavity, *Phys. Rev. Research* **2**, 012076(R) (2020).
- [16] C.-R. Mann and E. Mariani, Topological transitions induced by cavity-mediated interactions in photonic valley-Hall metasurfaces, [arXiv:2010.01636](https://arxiv.org/abs/2010.01636).
- [17] C.-R. Mann, S. A. Horsley, and E. Mariani, Tunable pseudo-magnetic fields for polaritons in strained metasurfaces, *Nat. Photonics* **14**, 669 (2020).
- [18] S. Diehl, E. Rico, M. A. Baranov, and P. Zoller, Topology by dissipation in atomic quantum wires, *Nat. Phys.* **7**, 971 (2011).
- [19] G. Goldstein and C. Chamon, Decay rates for topological memories encoded with Majorana fermions, *Phys. Rev. B* **84**, 205109 (2011).
- [20] J. C. Budich, S. Walter, and B. Trauzettel, Failure of protection of Majorana based qubits against decoherence, *Phys. Rev. B* **85**, 121405 (2012).
- [21] L. Mazza, M. Rizzi, M. D. Lukin, and J. I. Cirac, Robustness of quantum memories based on Majorana zero modes, *Phys. Rev. B* **88**, 205142 (2013).
- [22] C.-E. Bardyn, M. A. Baranov, C. V. Kraus, E. Rico, A. İmamoğlu, P. Zoller, and S. Diehl, Topology by dissipation, *New J. Phys.* **15**, 085001 (2013).
- [23] H. Z. Shen, W. Wang, and X. X. Yi, Hall conductance and topological invariant for open systems, *Sci. Rep.* **4**, 1 (2014).
- [24] Y. Hu, Z. Cai, M. A. Baranov, and P. Zoller, Majorana fermions in noisy Kitaev wires, *Phys. Rev. B* **92**, 165118 (2015).
- [25] D. Linzner, L. Wawer, F. Grusdt, and M. Fleischhauer, Reservoir-induced Thouless pumping and symmetry-protected topological order in open quantum chains, *Phys. Rev. B* **94**, 201105 (2016).
- [26] D. V. Else, P. Fendley, J. Kemp, and C. Nayak, Prethermal Strong Zero Modes and Topological Qubits, *Phys. Rev. X* **7**, 041062 (2017).
- [27] A. Carollo, B. Spagnolo, and D. Valenti, Uhlmann curvature in dissipative phase transitions, *Sci. Rep.* **8**, 9852 (2018).
- [28] M. J. Kastoryano and M. S. Rudner, Topological transport in the steady state of a quantum particle with dissipation, *Phys. Rev. B* **99**, 125118 (2019).
- [29] H. Weisbrich, W. Belzig, and G. Rastelli, Decoherence and relaxation of topological states in extended quantum Ising models, *SciPost Phys.* **6**, 37 (2019).
- [30] A. Carollo, D. Valenti, and B. Spagnolo, Geometry of quantum phase transitions, *Phys. Rep.* **838**, 1 (2020).
- [31] Y.-W. Huang, P.-Y. Yang, and W.-M. Zhang, Quantum theory of dissipative topological systems, *Phys. Rev. B* **102**, 165116 (2020).
- [32] C. Gneiting, A. Koottandavida, A. V. Rozhkov, and F. Nori, Unraveling the topology of dissipative quantum systems, [arXiv:2007.05960](https://arxiv.org/abs/2007.05960).
- [33] C. Leefmans, A. Dutt, J. Williams, L. Yuan, M. Parto, F. Nori, S. Fan, and A. Marandi, Photonic topological dissipation in a time-multiplexed resonator network, [arXiv:2104.05213](https://arxiv.org/abs/2104.05213).
- [34] M. Atala, M. Aidelsburger, J. T. Barreiro, D. Abanin, T. Kitagawa, E. Demler, and I. Bloch, Direct measurement of the Zak phase in topological Bloch bands, *Nat. Phys.* **9**, 795 (2013).
- [35] D.-W. Zhang, Y.-Q. Zhu, Y. X. Zhao, H. Yan, and S.-L. Zhu, Topological quantum matter with cold atoms, *Adv. Phys.* **67**, 253 (2018).
- [36] N. R. Cooper, J. Dalibard, and I. B. Spielman, Topological bands for ultracold atoms, *Rev. Mod. Phys.* **91**, 015005 (2019).
- [37] T. Ozawa, H. M. Price, A. Amo, N. Goldman, M. Hafezi, L. Lu, M. C. Rechtsman, D. Schuster, J. Simon, O. Zilberberg, and I. Carusotto, Topological photonics, *Rev. Mod. Phys.* **91**, 015006 (2019).
- [38] T. Ohta, S. Tanaka, I. Danshita, and K. Totsuka, Topological and dynamical properties of a generalized cluster model in one dimension, *Phys. Rev. B* **93**, 165423 (2016).
- [39] W. Nie, F. Mei, L. Amico, and L. C. Kwek, Scaling of geometric phase versus band structure in cluster-Ising models, *Phys. Rev. E* **96**, 020106(R) (2017).
- [40] Y. Che, C. Gneiting, T. Liu, and F. Nori, Topological quantum phase transitions retrieved through unsupervised machine learning, *Phys. Rev. B* **102**, 134213 (2020).
- [41] S. Bravyi, M. B. Hastings, and S. Michalakis, Topological quantum order: Stability under local perturbations, *J. Math. Phys. (N.Y.)* **51**, 093512 (2010).
- [42] M. Hafezi, E. A. Demler, M. D. Lukin, and J. M. Taylor, Robust optical delay lines with topological protection, *Nat. Phys.* **7**, 907 (2011).
- [43] M. Cheng, R. M. Lutchyn, and S. Das Sarma, Topological protection of Majorana qubits, *Phys. Rev. B* **85**, 165124 (2012).
- [44] I. Mondragon-Shem, T. L. Hughes, J. Song, and E. Prodan, Topological Criticality in the Chiral-Symmetric AIII Class at Strong Disorder, *Phys. Rev. Lett.* **113**, 046802 (2014).
- [45] C. Poli, M. Bellec, U. Kuhl, F. Mortessagne, and H. Schomerus, Selective enhancement of topologically induced interface states in a dielectric resonator chain, *Nat. Commun.* **6**, 6710 (2015).
- [46] O. Balabanov and H. Johannesson, Robustness of symmetry-protected topological states against time-periodic perturbations, *Phys. Rev. B* **96**, 035149 (2017).
- [47] T. Liu, Y.-R. Zhang, Q. Ai, Z. Gong, K. Kawabata, M. Ueda, and F. Nori, Second-Order Topological Phases in Non-Hermitian Systems, *Phys. Rev. Lett.* **122**, 076801 (2019).

- [48] Y. Wang, Y.-H. Lu, F. Mei, J. Gao, Z.-M. Li, H. Tang, S.-L. Zhu, S. Jia, and X.-M. Jin, Direct Observation of Topology from Single-Photon Dynamics, *Phys. Rev. Lett.* **122**, 193903 (2019).
- [49] W. Nie, Z. H. Peng, F. Nori, and Y.-X. Liu, Topologically Protected Quantum Coherence in a Superatom, *Phys. Rev. Lett.* **124**, 023603 (2020).
- [50] M. Gong, G. Chen, S. Jia, and C. Zhang, Searching for Majorana Fermions in 2D Spin-Orbit Coupled Fermi Superfluids at Finite Temperature, *Phys. Rev. Lett.* **109**, 105302 (2012).
- [51] O. Viyuela, A. Rivas, and M. A. Martin-Delgado, Uhlmann Phase as a Topological Measure for One-Dimensional Fermion Systems, *Phys. Rev. Lett.* **112**, 130401 (2014).
- [52] Z. Huang and D. P. Arovas, Topological Indices for Open and Thermal Systems Via Uhlmann's Phase, *Phys. Rev. Lett.* **113**, 076407 (2014).
- [53] B. Monserrat and D. Vanderbilt, Temperature Effects in the Band Structure of Topological Insulators, *Phys. Rev. Lett.* **117**, 226801 (2016).
- [54] C.-E. Bardyn, L. Wawer, A. Altland, M. Fleischhauer, and S. Diehl, Probing the Topology of Density Matrices, *Phys. Rev. X* **8**, 011035 (2018).
- [55] R. Unanyan, M. Kiefer-Emmanouilidis, and M. Fleischhauer, Finite-Temperature Topological Invariant for Interacting Systems, *Phys. Rev. Lett.* **125**, 215701 (2020).
- [56] M. McGinley and N. R. Cooper, Fragility of time-reversal symmetry protected topological phases, *Nat. Phys.* **16**, 1181 (2020).
- [57] H.-P. Breuer and F. Petruccione, *The Theory of Open Quantum Systems* (Oxford University Press, New York, 2002).
- [58] See the Supplemental Material at <http://link.aps.org/supplemental/10.1103/PhysRevLett.127.250402> for additional details about the derivation of the master equation, environment-induced topological phase transition, topological protection of quantum coherence, and experimental scheme for detecting the dissipative topological phase transition.
- [59] Y. Chen, C. Neill, P. Roushan, N. Leung, M. Fang, R. Barends, J. Kelly, B. Campbell, Z. Chen, B. Chiaro, A. Dunsworth, E. Jeffrey, A. Megrant, J. Y. Mutus, P. J. J. O'Malley, C. M. Quintana, D. Sank, A. Vainsencher, J. Wenner, T. C. White *et al.*, Qubit Architecture with High Coherence and Fast Tunable Coupling, *Phys. Rev. Lett.* **113**, 220502 (2014).
- [60] L. Knöll, S. Scheel, and D.-G. Welsch, QED in dispersing and absorbing media, [arXiv:quant-ph/0006121](https://arxiv.org/abs/quant-ph/0006121).
- [61] H. T. Dung, L. Knöll, and D.-G. Welsch, Resonant dipole-dipole interaction in the presence of dispersing and absorbing surroundings, *Phys. Rev. A* **66**, 063810 (2002).
- [62] D. Dzsotjan, A. S. Sørensen, and M. Fleischhauer, Quantum emitters coupled to surface plasmons of a nanowire: A Green's function approach, *Phys. Rev. B* **82**, 075427 (2010).
- [63] A. Gonzalez-Tudela, D. Martín-Cano, E. Moreno, L. Martín-Moreno, C. Tejedor, and F. J. Garcia-Vidal, Entanglement of Two Qubits Mediated by One-Dimensional Plasmonic Waveguides, *Phys. Rev. Lett.* **106**, 020501 (2011).
- [64] D. Martín-Cano, A. González-Tudela, L. Martín-Moreno, F. J. García-Vidal, C. Tejedor, and E. Moreno, Dissipation-driven generation of two-qubit entanglement mediated by plasmonic waveguides, *Phys. Rev. B* **84**, 235306 (2011).
- [65] G. Angelatos and S. Hughes, Entanglement dynamics and Mollow nonuplets between two coupled quantum dots in a nanowire photonic-crystal system, *Phys. Rev. A* **91**, 051803 (2015).
- [66] A. Asenjo-Garcia, J. D. Hood, D. E. Chang, and H. J. Kimble, Atom-light interactions in quasi-one-dimensional nanostructures: A Green's-function perspective, *Phys. Rev. A* **95**, 033818 (2017).
- [67] S. A. H. Gangaraj, G. W. Hanson, and M. Antezza, Robust entanglement with three-dimensional nonreciprocal photonic topological insulators, *Phys. Rev. A* **95**, 063807 (2017).
- [68] A. Asenjo-Garcia, M. Moreno-Cardoner, A. Albrecht, H. J. Kimble, and D. E. Chang, Exponential Improvement in Photon Storage Fidelities Using Subradiance and Selective Radiance in Atomic Arrays, *Phys. Rev. X* **7**, 031024 (2017).
- [69] P. Doyeux, S. A. H. Gangaraj, G. W. Hanson, and M. Antezza, Giant Interatomic Energy-Transport Amplification with Nonreciprocal Photonic Topological Insulators, *Phys. Rev. Lett.* **119**, 173901 (2017).
- [70] T. Shi, D. E. Chang, and J. I. Cirac, Multiphoton-scattering theory and generalized master equations, *Phys. Rev. A* **92**, 053834 (2015).
- [71] G. Calajó, F. Ciccarello, D. Chang, and P. Rabl, Atom-field dressed states in slow-light waveguide QED, *Phys. Rev. A* **93**, 033833 (2016).
- [72] M. Mirhosseini, E. Kim, X. Zhang, A. Sipahigil, P. B. Dieterle, A. J. Keller, A. Asenjo-Garcia, D. E. Chang, and O. Painter, Cavity quantum electrodynamics with atom-like mirrors, *Nature (London)* **569**, 692 (2019).
- [73] P. Y. Wen, K.-T. Lin, A. F. Kockum, B. Suri, H. Ian, J. C. Chen, S. Y. Mao, C. C. Chiu, P. Delsing, F. Nori, G.-D. Lin, and I.-C. Hoi, Large Collective Lamb Shift of Two Distant Superconducting Artificial Atoms, *Phys. Rev. Lett.* **123**, 233602 (2019).
- [74] M. Zanner, T. Orell, C. M. Schneider, R. Albert, S. Oleschko, M. L. Juan, M. Silveri, and G. Kirchmair, Coherent control of a symmetry-engineered multi-qubit dark state in waveguide quantum electrodynamics, [arXiv:2106.05623](https://arxiv.org/abs/2106.05623).
- [75] W. P. Su, J. R. Schrieffer, and A. J. Heeger, Solitons in Polyacetylene, *Phys. Rev. Lett.* **42**, 1698 (1979).
- [76] J. K. Asbóth, L. Oroszlány, and A. Pályi, *A Short Course on Topological Insulators* (Springer, New York, 2016).
- [77] N. C. Murphy, R. Wortis, and W. A. Atkinson, Generalized inverse participation ratio as a possible measure of localization for interacting systems, *Phys. Rev. B* **83**, 184206 (2011).
- [78] W. Nie, T. Shi, F. Nori, and Y.-X. Liu, Topology-Enhanced Nonreciprocal Scattering and Photon Absorption in a Waveguide, *Phys. Rev. Applied* **15**, 044041 (2021).

- [79] V. V. Albert, B. Bradlyn, M. Fraas, and L. Jiang, Geometry and Response of Lindbladians, *Phys. Rev. X* **6**, 041031 (2016).
- [80] F. Minganti, A. Biella, N. Bartolo, and C. Ciuti, Spectral theory of Liouvillians for dissipative phase transitions, *Phys. Rev. A* **98**, 042118 (2018).
- [81] F. Minganti, A. Miranowicz, R. W. Chhajlany, and F. Nori, Quantum exceptional points of non-Hermitian Hamiltonians and Liouvillians: The effects of quantum jumps, *Phys. Rev. A* **100**, 062131 (2019).
- [82] S. Lieu, M. McGinley, and N. R. Cooper, Tenfold Way for Quadratic Lindbladians, *Phys. Rev. Lett.* **124**, 040401 (2020).
- [83] T.-S. Deng, L. Pan, Y. Chen, and H. Zhai, Stability of Time-Reversal Symmetry Protected Topological Phases, *Phys. Rev. Lett.* **127**, 086801 (2021).